J Therm Spray Tech
https://doi.org/10.1007/s11666-024-01758-8

ORIGINAL RESEARCH ARTICLE

A Comparative Study on Wear Resistance of Cold-Sprayed Aluminum/Quasicrystal Composite Coatings

Reza Jafari[1] · Jan Cizek[2,3] · Frantisek Lukac[2] · Ladislav Cvrcek[3] · Matej Buril[3] · Jan Walter[3] · Mari Honkanen[4] · Minnamari Vippola[1,4] · Heli Koivuluoto[1]

Submitted: 9 October 2023 / in revised form: 31 January 2024 / Accepted: 5 March 2024

Abstract Cold spray (CS) technology has proven a great potential in the production of composite coatings, enabling the production of materials with superior qualities such as enhanced tribological behavior. This study aims to investigate the tribological properties of CS Al-based composite coatings reinforced by quasicrystalline (QC) particles. Two different Al alloys were used as the matrix, AA 6061 and AA 2024, and mixed with Al-based QC particles (Al-Cr-Fe-Cu) at different Al/QC ratios. A room-temperature ball-on-disc test was then used to evaluate the wear resistance of the composite CS coatings in air and compared to those of the non-reinforced Al alloy CS coatings as well as a cast counterpart (AA 6061-T6). We have demonstrated that CS could be employed to produce thick and dense Al-QC composites that can retain up to about 50 wt.% QC reinforcement in the structure. The incorporation of the QC particles increased the wear resistance by a factor of 7.

Keywords characterization · gas dynamic cold spray (GDCS) · light alloys · particle reinforcement · quasicrystalline · tribology

Introduction

The cold spray (CS) technology offers a fast and reliable coatings production route with an additional application also for repairs and additive manufacturing of components (Ref 1, 2). The high-speed impact of feedstock powder particles accelerated toward the substrate provides the energy required for their deformation. If the kinetic energy of particles is high enough, they have the potential to undergo deformation and form bonds with the substrate material or with each other, whether through mechanisms like mechanical interlocking or metallurgical bonding. This can initiate the coating buildup on a target surface (Ref 3). The whole CS deposition process takes place in the solid state as the temperature of the particles in the gas stream remains considerably below their melting point. Consequently, the phases in the original feedstock materials are typically preserved in the final coating, in contrast to high temperature thermal spray processes (Ref 3-5). These features highlight CS as a solution for deposition of heat-sensitive materials.

This article is an invited paper selected from presentations at the 2023 International Thermal Spray Conference, held May 22-25, 2023, in Québec City, Canada, and has been expanded from the original presentation. The issue was organized by Giovanni Bolelli, University of Modena and Reggio Emilia (Lead Editor); Emine Bakan, Forschungszentrum Jülich GmbH; Partha Pratim Bandyopadhyay, Indian Institute of Technology, Karaghpur; Šárka Houdková, University of West Bohemia; Yuji Ichikawa, Tohoku University; Heli Koivuluoto, Tampere University; Yuk-Chiu Lau, General Electric Power (Retired); Hua Li, Ningbo Institute of Materials Technology and Engineering, CAS; Dheepa Srinivasan, Pratt & Whitney; and Filofteia-Laura Toma, Fraunhofer Institute for Material and Beam Technology.

✉ Reza Jafari
reza.jafari@tuni.fi

[1] Materials Science and Environmental Engineering, Faculty of Engineering and Natural Sciences, Tampere University, 589, 33104 Tampere, Finland

[2] Institute of Plasma Physics of the Czech Academy of Sciences, Prague, Czech Republic

[3] Department of Materials Engineering, Faculty of Mechanical Engineering, Czech Technical University in Prague, Prague, Czech Republic

[4] Tampere Microscopy Center, Tampere University, 692, 33014 Tampere, Finland

Published online: 25 March 2024

Indeed, cold spraying has been extensively used in deposition of Al and Al alloys while successfully preventing their oxidation (Ref 6). Despite the increasing demand and variety of Al alloy applications, their tribological characteristics might still present a bottleneck (Ref 7). This issue can be resolved by developing metal matrix composites (MMC) through the addition of reinforcing phases/particles into the CS coating structure (Ref 8, 9). Hard phases such as diamond, SiC, WC, or Al_2O_3, have been demonstrated to provide significant mechanical and tribological improvements to cold-sprayed metallic coatings, being used as reinforcement (Ref 4, 10-13). The beneficial effect of the hard/heavy particle addition does not stem only from their inherent mechanical or tribological properties, but also includes additional synergistic factors, such as more pronounced deformation of the CS coatings via tamping of the previously deposited materials, leading to a reduction of porosity or grain refinement. As an outcome, e.g., the wear behavior may be improved (Ref 13-15). An alternative route to enhance the tribological properties is through incorporation of low friction materials into the coatings. This approach was observed in CS composite systems such as Inconel 718-graphene nanoplates (Ref 16) and Cu-MoS_2 (Ref 17), where the wear rate and coefficient of friction have been reduced due to the intrinsic lubricity of the graphene and MoS_2, respectively. Combining the hardness of WC and low friction of MoS_2 in hybrid reinforced Cu matrix with MoS_2-WC has resulted to even better stability of coefficient of friction and lower wear rate compared to the CS Cu-MoS_2 composite coating (Ref 18). In particular for CS Al-based MMC, strengthening the structure using ceramics such as SiC and Al_2O_3 premixed with various Al alloys was promising for wear damage reduction (Ref 19-22). As reviewed in Ref 9, 23, this approach can increase the potential of the Al-based coatings to be used in applications where the tribological characteristics hold significant importance such as engine cylinders, disc brakes, piston crowns, rotating blade sleeves, brake drums, gear parts, crankshafts, and drive shafts.

Ever since the discovery of quasicrystalline (QC) materials in 1984 (Ref 24), their potential applications have been widely investigated (Ref 25, 26). As an intermetallic complex compound, high hardness and reduced friction are the features that highlight the QC tribological properties (Ref 25, 27-29). Deposition of QC-based coatings by thermal spray technologies such as high-velocity oxy-fuel (HVOF) and high-velocity air-fuel (HVAF) have already shown their notable benefits in enhancing wear resistance (Ref 30, 31). However, their inherent brittleness remains a technical challenge for the industrial applications if used standalone (Ref 32, 33). Therefore, it was suggested to employ QC as the reinforcing phase in composite structures instead (Ref 34, 35). This idea has been implemented in several studies focused on composite fabrication, such as successful reinforcement of an Al matrix by nano Al-Cu-Fe through mechanical milling and spark plasma sintering (Ref 36), or cold spraying of Al-Cr-Mn-Co-Zr powders containing QC phase in a form of nanodispersoid (Ref 37). Particularly from cold spraying standpoint, successful fabrication of QC-reinforced MMC yielded improved characteristics such as higher pitting corrosion resistance (Ref 37), extended thermo-mechanical durability (Ref 38), and increased hydrophobicity (Ref 39). However, in terms of tribological performance, to the best of our knowledge, only limited number of studies on cold spraying of QC-containing composites can be found: superior wear behavior of cold-sprayed CuSn matrix with Al-Cu-Fe-B particles (Ref 40) and Ti matrix with Al-Cr-Fe particles (Ref 41) compared to the their non-reinforced counterparts. In both cases, the optimal resistance against wear was achieved at a relatively low QC content (11.5 vol.% in the coating and 20 wt.% in the initial feedstock, respectively). Further increase of the reinforcement content, up to 20.5 vol.% for the former and up to 30 wt.% for the latter, led to a wear resistance decline. Even though CS Al composite coatings possess appealing features that have the potential to increase their application potential in industrial markets, we have not found a dedicated study on wear performance assessment of QC-reinforced Al alloys. Thus, the resistance to wear of Al-based matrix composite coatings with varying proportion of QC remains unknown and interesting for exploration.

In our previous work (Ref 39), during artificial defect formation on the coating surfaces by abrasive particles, the composite coatings showed a higher resistance against volume loss by erosion compared to non-reinforced CS AA 6061 coatings. Following up on our previous study (Ref 39), this work aimed to investigate, quantify, and compare the wear behavior and properties of several CS Al-based composite coatings reinforced by QC particles. Two Al-based alloys, AA 6061 and AA 2024, were mixed with the Al-based QC powders of two different particle sizes at different mutual ratios. Sliding wear test, hardness, and basic microstructural characterization were the criteria used to assess and contextualizing the wear performance of the CS Al-QC composite coatings on the benchmark of well-known bulk metallurgical Al alloy and CS Al alloys. Even though the QC generally possess a high hardness, thick and dense composite coatings were successfully deposited using the CS process and their beneficial effect in increasing resistance against wear was quantified.

Experimental

The QC feedstock material used in this work was an atomized Al-based quasicrystalline powder (Al-Cr-Fe-Cu, Cristome A1, Saint-Gobain Coating Solutions, Avignon,

France). More details regarding its chemical composition can be found in our previous research (Ref 39). To comprehend the anticipated effect of the QC particle size, two particle size distributions were used: − 53 + 20 µm sieve range referred to as the coarse (C), and − 30 + 10 µm sieve range referred to as the fine (F). The actual particle size range of all powders was quantified using laser analysis (Mastersizer 3000, Malvern, UK). Gas-atomized AA 6061 (with nominal particle size of − 53 + 15 µm) powder from ECKART TLS GmbH (Bitterfeld-Wolfen, Germany) and AA 2024 (with nominal particle size of − 45 + 15 µm) powder from TLS Technik GmbH (Bitterfeld, Germany) were used to formulate the feedstock powder blends (Table 1). These were prepared by physical mixing of the desired volumetric ratio of the QC and the AA powders.

The substrates were 3-mm AA 6082 plates. They were grit blasted prior to spraying (alumina grit, average size ~ 690 µm) and fixed vertically at a constant 40 mm standoff distance from the cold spray nozzle. High-pressure PCS-100 (Plasma Giken Co., Ltd., Saitama, Japan) cold spray system with N_2 as the propeller gas was used to deposit the coatings. The process parameters (Table 1) were optimized in our earlier trials and aimed to reach the coating thicknesses in range of 300-500 µm.

The tribological properties were tested using the TRB-S-CE-0000 tribometer (CSM Instruments, Brüttelen, Switzerland) in a ball-on-disk arrangement. For each type of sample, two tribological tests were performed. Before the tests, the sample surfaces were mechanically ground using silicon carbide papers up to P4000 grit size (Struers, Switzerland). Subsequently, the sample surfaces were polished using 0.05 µm colloidal silica (Leco, USA) to a mirror finish. An Al_2O_3 ball with a diameter of 6 mm was used as a friction counterpart on polished surface of the coatings. To broaden our understanding of the results and contextualize the wear resistance of the CS coatings, a metallurgical AA 6061-T6 bulk was used in the wear tests as the reference. The surfaces of the samples and the Al_2O_3 balls were cleaned with acetone prior to each testing. A normal load of 1 N was used, and the linear sliding speed was set to 50 mm/s. The tests were performed for 5000 laps at a turning radius of 5 mm in air corresponding to a total distance of 157 m. The coefficient of friction, μ, was calculated from the ratio of the tangential friction force and the normal force. After the tests, the surface of the Al_2O_3 balls and the wear tracks were analyzed using a DSX1000 digital microscope (Olympus, Japan). To ensure the repeatability, two tribological tests were performed on each type of materials. In more detail, the wear track profiles were further analyzed using an optical 3D profilometer, Alicona InfiniteFocus G5 (Alicona Imaging GmbH, Graz, Austria). Following the method of Archard, the specific wear rate was calculated as $k = V / F{\cdot}s$ (Ref 42), where k ($mm^3/N{\cdot}m$) is the wear rate, V (mm^3) is the wear volume, F (N) is the normal load, and s (m) is the sliding distance. The net wear volume loss was obtained by integrating the depth profile along the whole length of wear tracks for each sample, using a VolumeMeasurement module in IF-MeasureSuite V 5.1 (Alicona Imaging GmbH, Graz, Austria). The robustness of the employed technique in considering all the height points inside the wear tracks leads to an accurate reading and reduces the variation and uncertainty of volume loss measurements.

The morphology of the feedstock materials, cross section of the CS coatings, and the wear tracks were analyzed by Zeiss ULTRA plus field emission scanning electron microscope (Carl Zeiss Microscopy GmbH, Jena, Germany) equipped with XMaxN energy-dispersive spectrometer (EDS, Oxford Instruments, Abingdon, UK). The cross sections were made by low-speed cutting followed by standard metallographic procedures. For cross-sectional observation of the sprayed coatings using backscattered electron detector (BSE) as well as the EDS analysis, an acceleration voltage of 10 kV was applied. To highlight the superficial features of the samples, the secondary electron (SE) imaging was used with the acceleration voltage reduced to 1-3 kV with the working distance close to

Table 1 Sample annotations, the respective feedstock composition, and CS process parameters used for the deposition. All QC contents are provided in volumetric %. The symbols p and T are the pressure and preheating temperature of N_2 used as the process gas

Annotation	Feedstock composition	CS process parameters					
		p (bar)	T (°C)	Step size (mm)	Feed (rpm)	CS gun traverse speed (m/min)	Coating layers
A	AA 6061	40	400	1	1.5	20	4
B	AA 2024	40	450	1	3	10	4
A-90C	AA 6061 + 90% coarse QC	20	450	1.5	3	5	3
A-50C	AA 6061 + 50% coarse QC	20	450	1.5	3	5	2
A-50F	AA 6061 + 50% fine QC	20	450	1.5	3	5	3
B-50C	AA 2024 + 50% coarse QC	20	450	1.5	3	5	3

5 mm. Analysis of the SEM images to determine porosity, thickness, and phase content was carried out on five individual coating cross sections, using ImageJ open-source software package (NIH, USA). The correlation of QC content within the composite coating and the corresponding feedstock was discussed accordingly. It is noteworthy to mention that the accurate calculation of the QC retention necessitates knowledge of deposition efficiency values, which were not measured during the cold spraying process in this study.

To measure the average hardness value of the coatings, Vickers indentation was used at 2 kgf load (equivalent to 19.61 N, FALCON 600, INNOVATEST Europe BV, Maastricht, The Netherlands). The indentation was performed on the polished surfaces with 10 s holding time per indent and repeated at least five times per each coating. The indent marks under the selected load were large enough to encounter several QC particles.

The phase composition of the samples was determined by the x-ray diffraction (XRD) method. The measurements were carried out using a D8 Discover vertical powder θ-θ diffractometer (Bruker AXS GmbH, Karlsruhe, Germany) using Cu K_α radiation with Ni K_β filter. The diffracted beam was detected by LynxEye 1D detector. Bragg–Brentano geometry was employed with 0.5° fixed divergent slit for the primary beam. The angular range (2θ) was changed from 15 to 120°, with a step size of 0.03° and the total time in each step of 192 s. The phase identification was done using X'Pert HighScore program (Malvern Panalytical, Malvern, UK) which accessed the PDF-4 + database of crystalline phases. Quantitative Rietveld refinement was performed in TOPAS V5, aiming at determination of the relative weight content of all identified phases (Ref 43). The quantification of the quasicrystal content in the sprayed coatings was less straightforward and required a calibration procedure for integral intensities calculation. This was realized using XRD measurement of artificially prepared mixtures of the Al alloy and the QC powders.

Results

Powder and Coating Characteristics

Figure 1 presents the particle morphology of the used feedstock powders. All four powders exhibited a spherical or semi-spherical particle morphology, with an infrequent presence of irregular particles. The QC particles exhibited a more corrugated, if slightly porous surface, visible particularly for the coarser particles. The presence of small satellites adhered to the bigger particles was detected, a consequence of the used gas atomization production method. Both AA 6061 and AA 2024 powders included a significant amount of relatively small, micron-sized particles along with the larger particles, indicating a broader

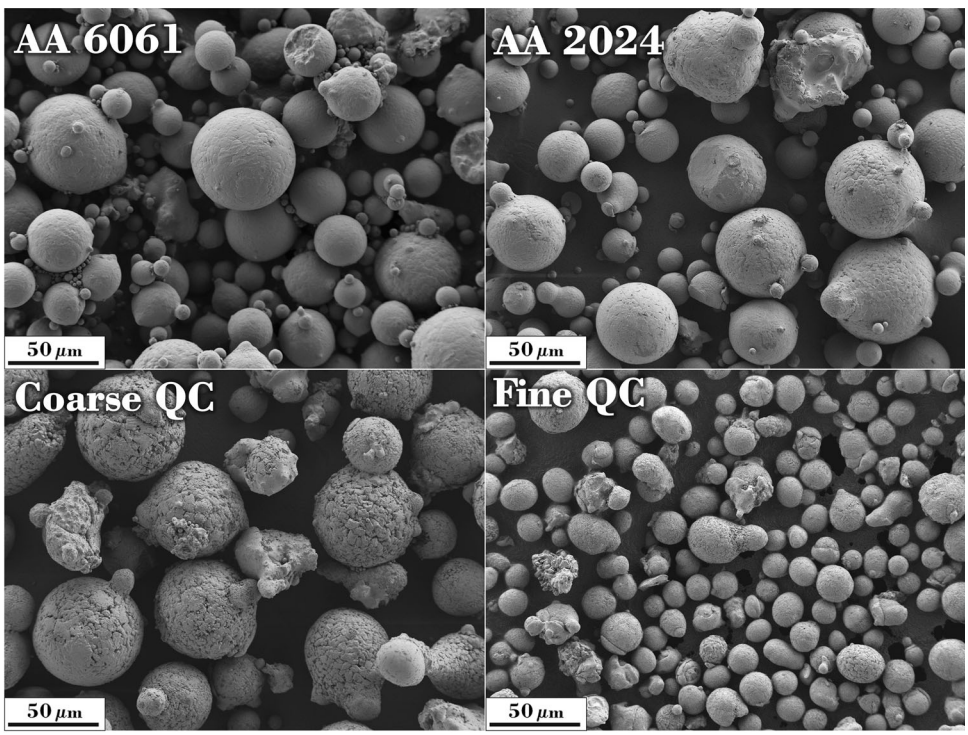

Fig. 1 SEM images (SE) showing the morphology of the used powder feedstock particles

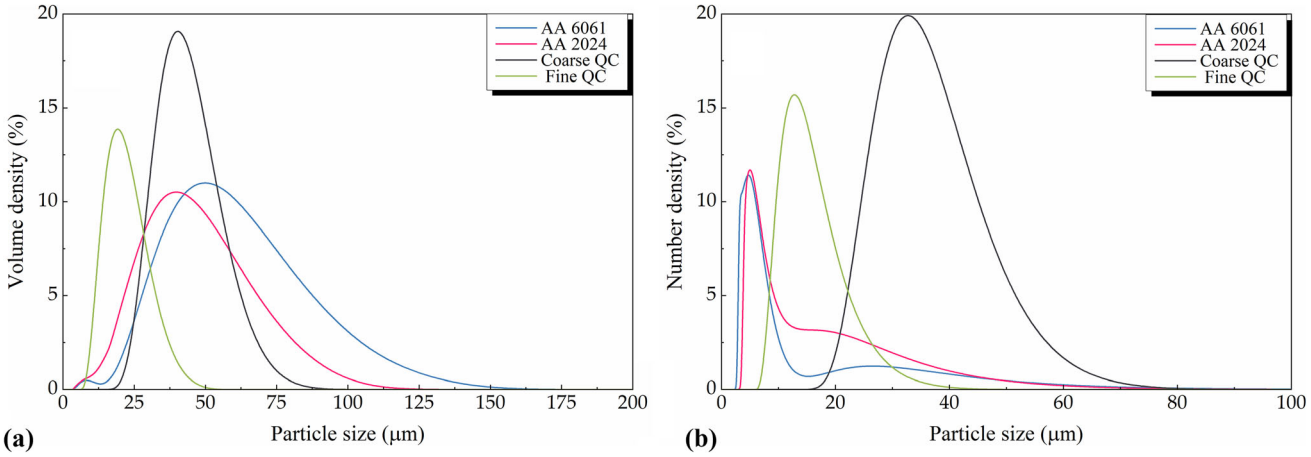

Fig. 2 Particle size distributions of the used powders. (a) Volume density versus particle size and (b) number density versus particle size. The difference between the volumetric and number densities is given by the presence of a significant number of small particles in the two Al alloy powders. Please mind the different ranges of the x-axes

distribution. This was confirmed by the laser analysis of the particle sizes (Fig. 2), where a big difference between volumetric (Fig. 2a) and number density (Fig. 2b) measurements was detected for these two powders (cf. the average volumetric and number density ranges of 27-89 μm versus 4-15 μm for AA 6061, and 19-69 μm versus 5-25 μm for AA 2024). Both powders also exhibited values higher than the nominal ranges indicated by the manufacturers. The two QC powders showed narrower distributions and, due to the absence of small particles, the difference between volumetric and number densities was not so pronounced (13-32 μm versus 10-22 μm for the fine QC, 31-59 μm versus 26-50 μm for the coarse QC). The ranges of both QC powders corresponded well to the used sieve ranges, testifying to good processability of the powder.

The cross section of the coatings described in Table 1 is presented in Fig. 3. Comparing the particle shapes in the coatings to their original geometry shown in Fig. 1, the Al alloy particles underwent significant deformation and flattened markedly in the deposition process. The deformation of the QC particles depended on their relative content in the coatings: for lower content, the QC particles tended to retain the original spherical morphology, with only limited and infrequent fragmentation. With increasing QC content, the particles clearly underwent an increased level of fragmentation, triggering an occurrence of small, standalone fragments in the coatings.

The two non-reinforced coatings, A and B, exhibited relatively higher levels of porosity, predominantly located at the particle boundaries (inset micrographs in Fig. 3). Importantly, no evident pore formation took place at the Al matrix-QC boundaries, testifying to the good coherence of the two phases. The coatings/Al-based substrate interfaces were bonded without visible clues of delamination or interfacial cracks.

Regardless of the Al matrix (gray color in BSE micrographs), the (white contrast) QC particles were homogeneously distributed through the entire coatings thickness, validating the applicability of the CS process for a successful composite coating formation. Due to the (anticipated) selective deposition efficiency, the QC particles content in the coatings decreased as compared to the initial feedstock (Table 2).

Increasing the QC content, the following phenomena might have been triggered as discussed in Ref 12: (i) hammering of the underlying structure and pore elimination, (ii) incorporation of the fragments from rebounded or cracked particles, and (iii) the soft phase interlocking and bonding to the fragments. Ultimately, these could lead to the observed deformation and fragmentation of the QC particles retained in the coatings; the inset image of A-90C in Fig. 3 represents a trapped fractured QC powder in the surrounding softer Al phase with highly deformed and refined grains. The tamping effect of the QC particles has evidently improved the bonding between Al particles as their interfaces were not easily detectable.

As shown in Fig. 4, the hardness of the composite coatings is higher than that of their non-reinforced counterparts. All CS composites with 50 vol.% QC in the powder feedstock were relatively hardened by + 20 to + 25% compared to the non-reinforced coatings, presumably due to the densification and pronounced work hardening induced by the tamping effect of the QC particles (Ref 20). Clearly, larger QC impact imposed more hammering to the structure. Further, increasing the coarse QC feedstock content from 50 to 90% led to a higher coating hardness. The T6 heat treatment and the higher density (absence of porosity) of the metallurgical bulk AA 6061 may account

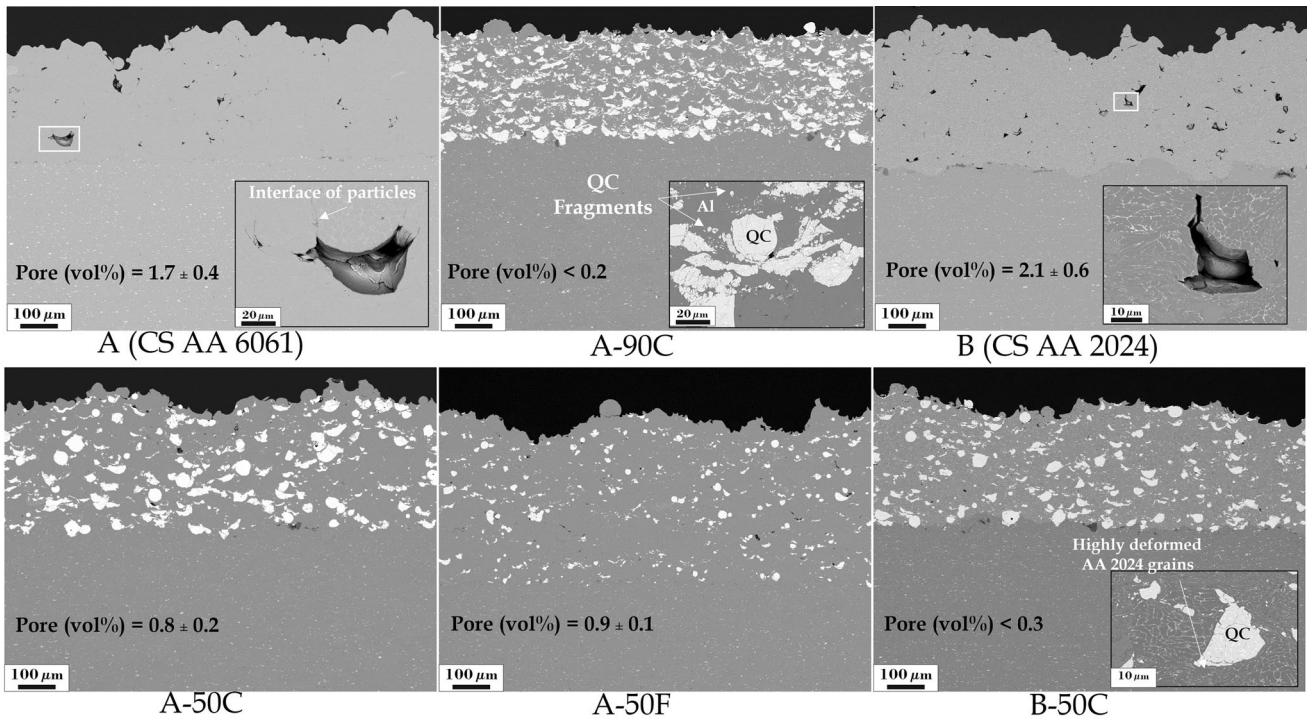

Fig. 3 Cross-sectional SEM (BSE) images of the as-sprayed coatings. The provided insets represent magnified views of the areas of interest. The porosity content was measured by image analysis of five different cross section views

Table 2 Composition of the feedstock powders, QC content from image analysis extended to volumetric value assuming the homogenous distribution of the phases in 3D, and QC content in the coatings as determined by XRD

Sample	QC in feedstock (vol.%)	QC in coating (vol.%) by image analysis	QC in coating (wt.%)
A-50C	50	21.4 ± 2.1	31
A-50F	50	8.4 ± 1.9	11
B-50C	50	18.3 ± 1.2	24
A-90C	90	42.9 ± 1.8	48

for the nearly 18% difference in the mean hardness as compared to the CS A coating.

In general, all AA 2024-based coatings have shown higher hardness values compared to those of their equivalent AA 6061 coatings. This effect is probably connected to the alloy composition, specifically the presence of higher Cu content in AA 2024, which enhances its strength and hardness by forming Cu-rich precipitates, while AA 6061 rich in Si and Fe with overall lower content is known for its better formability (Ref 44, 45).

The XRD analysis of the quasicrystalline powder confirmed it mostly comprises of an icosahedral phase isomorphous with the Al13-Cr3-Cu4 phase (PDF #00-048-1562, (Ref 46)). Since a quasicrystalline phase does not have a translational symmetry and therefore no unit cell available for the Rietveld quantification, the QC phase amounts in the coatings provided in Table 2 were calculated from integral intensities of selected major peaks of the icosahedral phase in the spectra (not presented here) normalized to the reference samples of mixed feedstock powders, as described in the experimental section. A minor content of crystalline, tetragonal Cu_2Al phase was recorded in the QC powders. From the results, several interesting conclusions can be drawn. First, the effectiveness of retaining the fine QC content in the coating structure was significantly lower when compared to retention of the coarse QC phase (cf. A-50F and A-50C in Table 2). This could potentially be attributed to the fact that the same number of retained larger particles yields a higher QC content when compared with the cumulative retained volume of the same number of fine particles. Second, comparing the A-50C and B-50C coatings, it seems that the AA 6061 alloy matrix is more efficient in retaining the quasicrystals in the composite. A possible reason might be

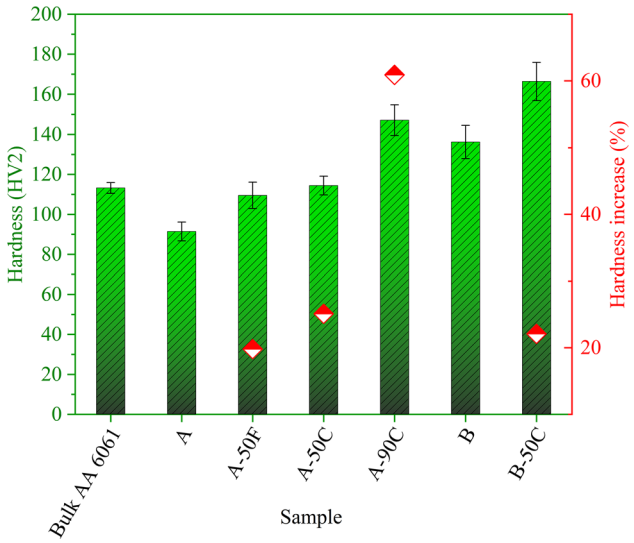

Fig. 4 The hardness of tested specimens (green bars) and the percentage hardness increase of the CS composite coatings with respect to their CS matrices (red scatter symbols) (Color figure online)

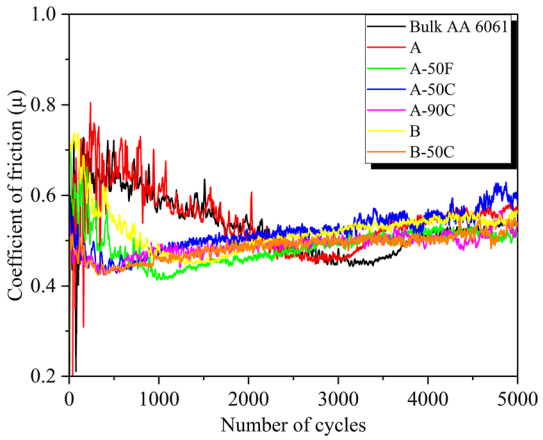

Fig. 5 The coefficients of friction of the samples tested against the Al_2O_3 ball

the lower hardness and higher formability of the AA 6061 as compared to that of AA 2024 (Ref 44, 45), enabling a higher deformation capacity for the QC particles incorporation. Third, increasing the QC content in the feedstock from 50 to 90 vol.% (40 percentage points increase) corresponds to an approximately + 21.5 percentage points rise in the coatings. This is associated with selective deposition efficiency; a higher QC content in the feedstock increases the probability of non-effective impacts (i.e., QC particles rebounding on QC particles), and in turn, the chance of QC loss during spraying is higher. To accurately quantify the retained QC in practice, it is crucial to consider the deposition efficiency (DE) values for Al-QC spraying. In the absence of absolute DE values, relative deposition efficiency of Al-QC can be qualitatively inferred from the thickness per pass, which is lower for A-90C (~113 μm/pass) compared to A-50C (~203 μm/pass). In the case of A-90C, it is likely that more feedstock is lost during cold spraying. Therefore, the actual decrease in retained QC fraction (from consumed feedstock to the developed coating) is presumably larger compared to A-50C.

Sliding Wear

The coefficient of friction (μ) and the wear rate of the samples were calculated by sliding of a 6 mm diameter Al_2O_3 ball counterpart over the polished sample surfaces. After the running-in phase, the average μ was in the range of 0.5-0.6 for all tested samples (Fig. 5). The coefficient of friction for the cast and cold-sprayed AA 6061 was almost the same. However, these two samples exhibited a much longer running-in phase that ultimately stabilized to lower values, compared to the other samples. A similar behavior was observed in testing of CS Al-nanodiamond composites (Ref 47). It is interesting to note that in that study, the coefficient of friction started from the lower values and increased during run-in phase after the heat treatment.

Figure 6 clearly indicates the effect of QC addition on the wear rate and wear track width of the tested coatings. The wear performance was evaluated from the wear track width first, where the beneficial effect of quasicrystals was confirmed. Both CS Al-based alloys, A and B, always had a larger wear, manifested by the greater wear track widths than the QC-reinforced composites. Aluminum component was wrapped on the ball in case of A, unlike the best preforming composite, A-90C, that there was no wrapping of the aluminum component on the ball (See supplementary materials S2). For the composite coatings, the run-in phase was shortened, and the resulting wear rates were several times lower.

Of the composite coatings, the A-50F had the highest wear rate and track width. One of the reasons could be the lowest actual QC content among the coatings, amounting to 11 wt.% only. As the amount of QC in the composite structure increased, the wear rate was expected to decrease. However, the recorded decrease was relatively small, not quite corresponding to the QC content increase.

Importantly, all composite structures showed wear rates lower than the precipitation-hardened bulk AA 6061-T6. As compared to the corresponding non-reinforced CS Al alloys, the wear resistance improvement of the A-90C sample was + 703%, a rather significant enhancement of the tribological properties. Further, the improvement was as high as + 586% for A-50C, + 312% for A-50F, and + 273% for B-50C. Comparison of these values

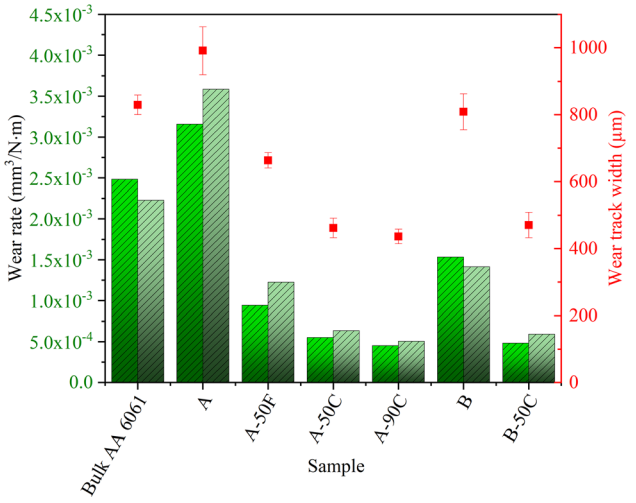

Fig. 6 The wear rates (bars, calculated for two samples) and the average wear tracks widths (red squares) of the tested materials. The corresponding 3D profiles and optical images of the wear tracks are available in the supplementary materials (S1) (Color figure online)

clearly indicated that the softer AA 6061 benefited more from the QC incorporation in the structure by CS.

The best and worst performing coating samples with the AA 6061 matrix, i.e., A-90C and A, were selected for a subsequent residual wear tracks characterization and compared to that of the bulk AA 6061-T6 sample. Figure 7 provides the corresponding micrographs and EDS analysis of the features observed on the studied wear track surfaces. The A-90C sample with the highest wear resistance had a significantly narrower wear region. The combination of several factors, such as high content of the harder QC particles, and the tamping-induced grain refinement and pore elimination triggered the remarkable decline of wear damage compared to Al alloy counterpart (Ref 13-15). The higher magnification micrographs presented in Fig. 7 contain evidence of a ductile deformation of the AA 6061 matrix as the governing factor in the wear mechanism. The agglomerated debris found locally inside the wear track was generally oxidized metallic elements as confirmed by the EDS results. Nevertheless, most of the wear tracks were composed of a smooth tribofilm with a localized detachment. Interestingly, no visible signs of the reinforcing particle pullouts were found in the observed regions, indicating a good coherence between the Al matrix and the QC particles. The EDS analysis from the smoother region showed Cu, Cr, and Fe signals, i.e., elements originally present in the QC particles. This would indicate either a surface exposure or subsurface presence of QC particles. An explanation for the lower coefficient of friction in the running-in period can be the low friction nature of the QC particles that are in contact with the Al_2O_3 ball before formation of the tribofilm and reaching the steady state. In contrast, the residual wear groove of the CS AA 6061 with the lowest wear resistance consisted of a spalled, Al-rich oxide tribofilm. As observed by SEM and the optical profilometer, the CS AA 6061 coating and AA 6061 bulk exhibited formation of parallel grooves inside the wear scar along the wear direction deeper than similar grooves formed on the composite samples. Here, the tribofilm consists of Al-rich oxides with local detachment, exposing the non-oxidized metal surface.

The wear track morphologies of samples B and B-50C were also investigated by SEM. The B-50C composite coating compared to non-reinforced CS AA 2024 (B) exhibited a narrower track as shown in Fig. 8. Likewise, reinforcing CS AA 2024 with coarse QCs has changed the wear track morphology due to alteration of wear mechanisms. Detachment of loose tribofilm, smearing and ploughing by ductile deformation and local presence of debris were the major features in the wear track of sample B. The wear track of B-50C mostly consisted of compacted and loose debris with limited signs of plastic flow and delamination in tribofilm compared to B. Such difference of the residual wear track morphology certifies the changing of wear mechanism toward having a more resistance in reinforced CS AA 2024 coating.

Discussion

The merits of the CS Al-QC composite coatings fabrication can be appreciated from several angles. Firstly, CS metallic coatings might have defects such as pores and discontinuity of the particle boundaries. Addition of the hard particles to the feedstock leads to hammering of the structure and consequently its densification (Ref 4) by exerting more deformation which can be alternatively achieved, e.g., by using costly and less accessible He as propeller gas (Ref 8, 48). Secondly, reinforced CS Al-based coatings can endow an enhanced wear resistance and an increased level of hardness which can extend their application in more demanding environments. Last but not least, the coating buildup solely from QC particles could have been highly fascinating because of their unconventional structure and properties. However, this is not viable by CS, as we have experienced in preliminary trials using a wide range of CS settings. Similar to efforts focusing on deposition of ceramic materials (Ref 49), the outcome was a $\sim$ 20-μm layer made of fractured QCs embedded into the substrate. As a solution, presence of a softer phase in the feedstock can assist QC retention during the coating buildup, while the QC intrinsic properties can still be exploited (Ref 34, 35, 39). These aspects are discussed as follows:

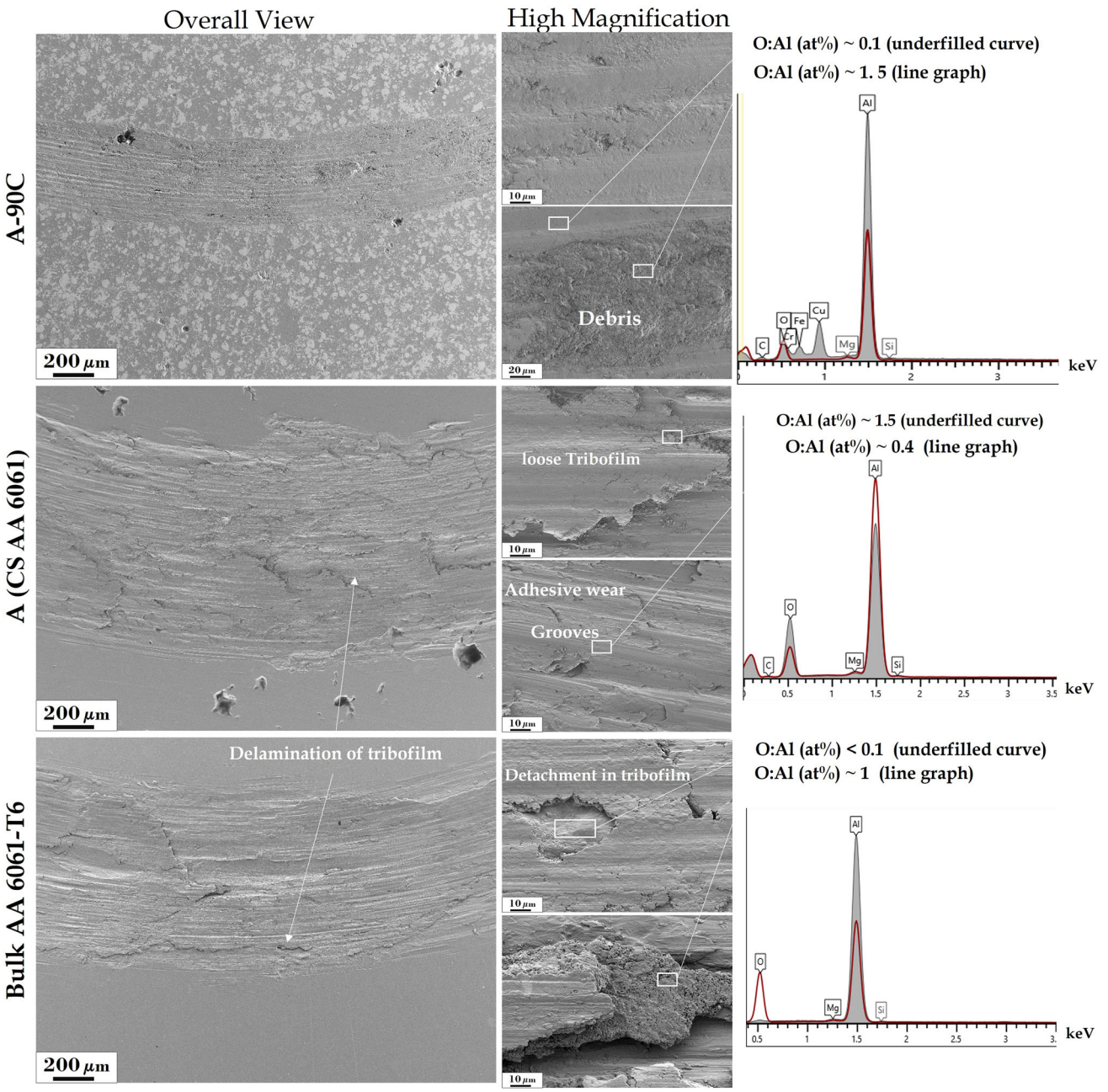

Fig. 7 A detailed wear track characterization of the best and worst wear-performing CS samples compared to the bulk metallurgical counterpart using SEM (SE) images and EDS. The atomic% ratio of O to Al for each graph is reported as a measure of oxidation

Composite Coating Formation

Increasing the coarse QC content in the starting feedstock from 0 to 50 and further up to 90 vol.% had a remarkable influence on the enhancement of CS AA 6061 coating structure through densification and increasing the hardness. These observed phenomena might be ascribed to the relationship between the QC content in the blended powder and the tamping effect exerted by the QC particles on the Al alloy particles. The limited deformability of QC particles (Ref 33) results in the higher level of energy transfer to the Al alloy particles. As a result, there is an increase in the level of particle deformation, leading to a densification of the coating and sealing of the pores and gaps inside the structure. Nevertheless, a trade-off exists; the higher the QC content in the feedstock mixture, the greater the likelihood of collision between hard and brittle QC particles that is expected to result in rebounding and fragmentation by shattering. To be specific, given the theoretical 50% chance of QC-QC collision in A-50C,

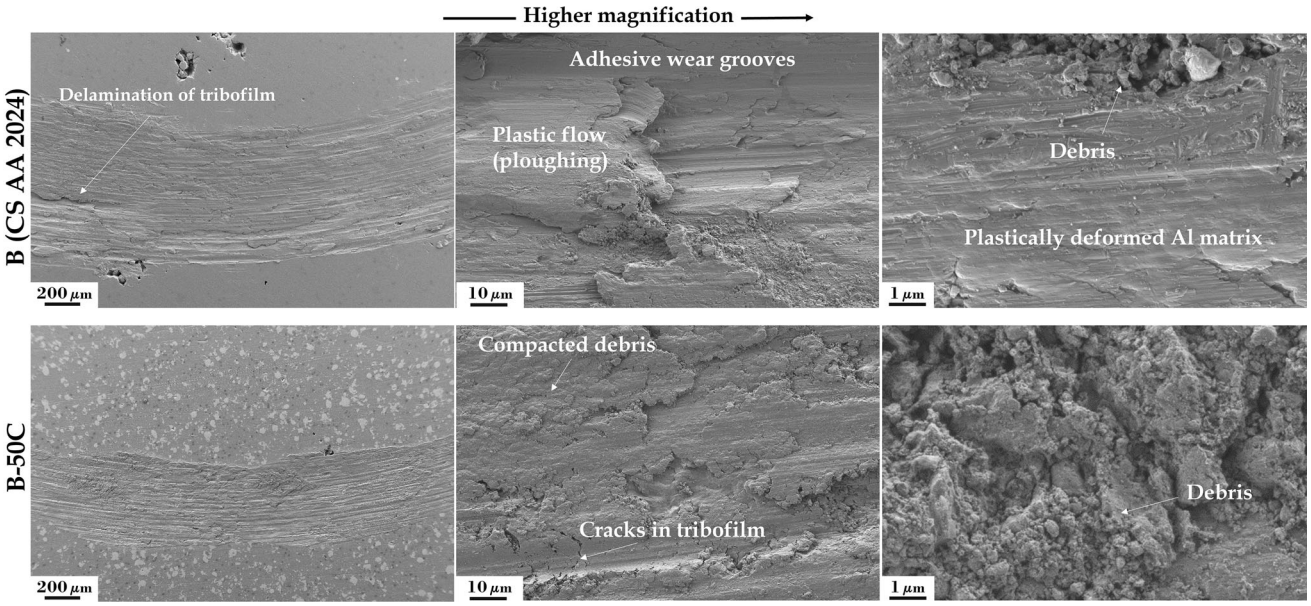

Fig. 8 Characterization of wear tracks of B (CS AA 2024) and B-50C (CS AA 2024 reinforced with QCs) using SEM (SE) images

some fragmentation is expected. However, in the case of A-90C, the probability of the QC particles impacting other QC particles is higher, yielding more visible and shattering-induced fragmentation, as reflected in the description of Fig. 3 in the Results section. Such a decline of reinforcement content is a known phenomenon for the cold-sprayed coatings deposited from blended feedstock of metallic matrix and hard particles such as Ti6Al4V-CoCr (Ref 12), Al-Al_2O_3 (Ref 19), Al alloy-SiC/B_4C (Ref 50), and Ni-WC (Ref 51), to name a few. In our study, the best performing composite coatings had a significantly higher QC content retained in the structure compared to other studies that have dealt with CS deposition of quasicrystals (Ref 40), even by using He as propeller gas (Ref 37). Our findings, however, have shown discrepancy with the earlier study (Ref 20), where the increase of reinforcement (Al_2O_3) beyond a certain level in the initial feedstock (optimum $\sim$ 30 wt.%) was not favored to an Al-based matrix due to the formation of more pores and microcavities in the vicinity of the reinforcements that compromise the coating mechanical properties. Likewise, as mentioned in the introduction section, CS Ti and CuSn matrices reinforced by QC have been reported to have a similar experience (Ref 40, 41), where the matrices were in general harder than the Al-based matrices used in our work. The smaller QC reinforcements seemed to have a smaller effect on tamping the structure compared to the larger QC particles that can possess a higher momentum upon impact (Ref 40).

A similar rationale can be assumed to justify the higher hardness of the composite coatings and their ranking; QC particles tamping exerts work hardening on the earlier deposited softer Al alloy particles, leading to higher dislocation density and grain refinement, similar to reports on CS Ti6Al4V-CoCr (Ref 12) or nanodispersoid strengthened CS AA 6061 (Ref 37). Both grain refinement and the QC content are potentially interesting features for the tribological properties enhancement. Moreover, the inherent higher hardness of the QCs might possibly assist in bearing a portion of the load imposed by the indenter. A noteworthy finding was that the similar hardness values of A-50F and A-50C do not correspond to the proportion of retained QCs in the structure. A potential reason might be the uniform distribution of fine QC and their fragments that shattered upon impact and dispersed throughout the cross section. The decrease in the average distance between the reinforcing particles, known as the mean free path, might potentially impose more limitations on the plastic deformation of the metal matrix (Ref 52). These dispersed fine QC and fragments may serve as obstacles against the dislocation movement and reduce the mean free path in matrices giving rise to hardness reading. Interestingly, A-50C and A-50mQC demonstrated higher wear resistance compared to B, even though B was relatively harder, highlighting the benefit of QC particles presence.

Comparing the A-50C and B-50C coatings, it seems that the AA 6061 alloy matrix is more efficient compared to AA 2024 in retaining the quasicrystals in the composite. The possible reason might be the lower hardness of the CS AA 6061 as compared to that of CS AA 2024, enabling a higher deformation capacity for the QC particles incorporation (Ref 44, 45).

Wear Performance

Due to the dynamic nature of the wear process and the diversity of its testing and characterization, it is often difficult to find wear test results of the materials of interest tested at identical conditions. This makes it difficult to compare the obtained absolute values and put them into the context of the materials used/tested elsewhere. To comprehend this, another approach is typically employed: testing an established material and setting it as an own benchmark (such as the CS Al alloys and bulk AA6061-T6 used in this work) and adopting a comparative approach. In particular, this is a required approach when evaluating less-known materials namely the developed CS Al-QC composite coatings in this study. For the ideal behavior of a wear resistant composite coating, the reinforced matrix is expected to retain the hard reinforcements in the composite structure throughout the cycles of the sliding load (Ref 4, 19, 40, 51). This is critical to avoid excessive abrasion that a pulled-out hard particle may cause as the third body. This issue was responsible for declining of the wear resistance of CS Al alloy-Al_2O_3 (Ref 20), by increasing the reinforcements ratio in the composite structure. A poor cohesion between the matrix and reinforcement phase could be a drawback of excessive reinforcement in the structure, facilitating particle pullout (Ref 40). Interestingly, such decline of wear resistance was not observed with increasing QC in the current test procedure. Neither the wear tracks nor the debris showed clear indication of large QC detachments in the QC-containing composites. However, the cycle of tribofilm formation and subsequent film detachment under the load of the counterface could be a contributing factor to the wear volume loss (Ref 53).

The CS and bulk aluminum alloys showed a similar ploughing wear track morphology with a smeared appearance identified as adhesive wear (Ref 47). Even though the adhesive wear was not observed on the surface of the Al_2O_3 ball counterpart, the morphology was similar to previous investigation on Al wear performance (Ref 47). The difference in wear behavior between the CS coatings and bulk materials could be potentially related to the presence of interparticle boundaries that might weaken the cohesion between the Al particles in CS coating under sliding load and higher density of the bulk, precipitation-hardened AA 6061-T6. On the other hand, less smearing in the wear track and a presence of oxidized metallic debris in the case of reinforced composite surfaces such as A-90C and B-50C would suggest an activation of the abrasive wear mechanism and suppressing the Al matrix extensive wear by adhesive wear (Ref 47). The reduction of adhesive wear and a transition to the abrasive wear resulted in a lower wearing of the composite coatings (Ref 53). Presence of angular reinforcement in the structure was reported to be more effective in incorporation of more reinforcement content in the structure (Ref 54), while there is a controversy in the effect of reinforcement morphology on wear and abrasion (Ref 19, 54-56). In the case of the CS Al-QC coatings presented in this work, due to shattering and fragmentation upon their impact, the originally spherical QC particles appeared to be irregular inside the composite coating structure. The formation of jagged features could endow a better interlocking and cohesion to the matrix (Ref 12); such features, in addition to reduction of mean free path and strengthening the structure, could presumably be reasons behind the lack of extensive abrasion due to the hard particle detachments during the sliding wear and the overall wear resistance enhancement.

Hardness often corresponds to wear resistance of ductile materials (Ref 20, 40, 57). Analogous to the effect of QC content on hardness, wear behavior of the composite coatings has shown a direct correlation to the QC content in the structure, but similar to the wear rate, the changes are not linearly proportional. An increase in the hardness value was achieved by increasing the QC ratio in starting feedstock, as seen from comparison of A-90C and A-50C. For the same samples, however, the enhancement of wear resistance was less significant even though A-90C was still the best performing coating in this comparison.

Despite earlier published results suggesting a low friction property for QC materials (Ref 28, 38), no remarkable reduction of the coefficient of friction was observed in our study. However, the run-in phase for QC-containing composite structure was accompanied with a lower coefficient of friction compared to the final state. We hypothesize here that in the earlier stages when there was a direct contact between the Al_2O_3 counterface and the QC phases, the low friction nature of the QC was the governing factor. In the later cycles when the oxidized surface encountered the Al_2O_3 ball, the μ value was stabilized in a close range for the tested materials.

Conclusions and Future Work

Cold-sprayed composite coatings made of two selected Al alloys reinforced by Al-based QC particles exhibited a remarkable enhancement of their wear resistance. The wear rate and wear track width values were significantly decreased by incorporation of the QC particles in the initial powder feedstock blends and consequently in the coatings. The best performing coating exhibited a remarkable 7 times improvement of the wear rate as opposed to the non-reinforced CS Al alloy. In this study, the QC incorporation was more beneficial with the AA 6061 matrix compared to the AA 2024 one, yielding higher wear resistance improvements. In addition, coarser QC particles were more

effective in improving the wear resistance. The microstructural studies along with the wear performance assessments indicated that the QC incorporation triggered the transition from adhesive wear to abrasive wear. In the upcoming works, there will be endeavors to reveal the wear mechanisms evolution through microstructural characterizations and investigate the Al-QC bonding in the CS coating composite structure.

Supplementary Information The online version contains supplementary material available at https://doi.org/10.1007/s11666-024-01758-8.

Acknowledgments The authors would like to express their gratitude to Mr. Jarkko Lehti and Mr. Anssi Metsähonkala of Tampere University for spraying the coating samples and Mr. Eero Helmi of Tampere University for help in experimental procedures. The IPP authors gratefully acknowledge the Czech Science Foundation project 22-14048S. Mr. Dominique Billieres of Saint-Gobain Coating Solutions is highly acknowledged for supporting this research. This work has used the facilities of Tampere Microscopy Center, Tampere, Finland. The Faculty of Engineering and Natural Sciences, Tampere University, is acknowledged by R.J. for the funding.

Funding Open access funding provided by Tampere University (including Tampere University Hospital).

References

1. X. Xie, S. Yin, R. Nirina Raoelison, C. Chen, C. Verdy, W. Li, G. Ji, Z. Ren, and H. Liao, Al Matrix Composites Fabricated by Solid-State Cold Spray Deposition: A Critical Review, *J. Mater. Sci. Technol.*, 2021, **86**, p 20-55. https://doi.org/10.1016/j.jmst.2021.01.026
2. S. Yin, P. Cavaliere, B. Aldwell, R. Jenkins, H. Liao, W. Li, and R. Lupoi, Cold Spray Additive Manufacturing and Repair: Fundamentals and Applications, *Addit. Manuf.*, 2017, **2018**(21), p 628-650.
3. T. Schmidt, F. Gärtner, H. Assadi, and H. Kreye, Development of a Generalized Parameter Window for Cold Spray Deposition, *Acta Mater.*, 2006, **54**(3), p 729-742.
4. H. Koivuluoto, G. Bolelli, A. Milanti, L. Lusvarghi, and P. Vuoristo, Microstructural Analysis of High-Pressure Cold-Sprayed Ni, NiCu and NiCu + Al2O3 Coatings, *Surf. Coat. Technol.*, 2015, **268**, p 224-229.
5. S. Yin, J. Cizek, J. Cupera, M. Hassani, X. Luo, R. Jenkins, Y. Xie, W. Li, and R. Lupoi, Formation Conditions of Vortex-like Intermixing Interfaces in Cold Spray, *Mater. Design*, 2021, **200**, p 109444.
6. D. Guo, M. Kazasidis, A. Hawkins, N. Fan, Z. Leclerc, D. MacDonald, A. Nastic, R. Nikbakht, R. Ortiz-Fernandez, S. Rahmati, M. Razavipour, P. Richer, S. Yin, R. Lupoi, and B. Jodoin, Cold Spray: Over 30 Years of Development Toward a Hot Future, *J. Therm. Spray Technol.*, 2022.
7. D. Cruz, M.Á. Garrido, Á. Rico, C.J. Múnez, and P. Poza, Wear Resistance of Cold Sprayed Al Alloys for Aeronautical Repairs, *Surf. Eng.*, 2019, **35**(4), p 295-303.
8. L. He and M. Hassani, A Review of the Mechanical and Tribological Behavior of Cold Spray Metal Matrix Composites, *J. Therm. Spray Tech.*, 2020, **29**(7), p 1565-1608. https://doi.org/10.1007/s11666-020-01091-w
9. N. Idusuyi and J.I. Olayinka, Dry Sliding Wear Characteristics of Aluminium Metal Matrix Composites: A Brief Overview, *J. Market. Res.*, 2019, **8**(3), p 3338-3346. https://doi.org/10.1016/j.jmrt.2019.04.017
10. R. Fernandez and B. Jodoin, Cold Spray Aluminum-Alumina Cermet Coatings: Effect of Alumina Morphology, *J. Therm. Spray Technol.*, 2019, **28**(4), p 737-755.
11. Q. Wang, K. Spencer, N. Birbilis, and M. Zhang, Surface & Coatings Technology the in Fl Uence of Ceramic Particles on Bond Strength of Cold Spray Composite Coatings on AZ91 Alloy Substrate, *Surf. Coat. Technol.*, 2010, **205**(1), p 50-56.
12. A.W.Y. Tan, J.Y. Lek, W. Sun, A. Bhowmik, I. Marinescu, P.J. Buenconsejo, Z. Dong, and E. Liu, Microstructure, Mechanical and Tribological Properties of Cold Sprayed Ti6Al4V-CoCr Composite Coatings, *Compos. Part B Eng.*, 2020, **202**, p 108280.
13. S.A. Alidokht and R.R. Chromik, Sliding Wear Behavior of Cold-Sprayed Ni-WC Composite Coatings: Influence OF WC Content, *Wear*, 2021, **477**, p 203792.
14. R. Nikbakht, M. Saadati, T.-S. Kim, M. Jahazi, H.S. Kim, and B. Jodoin, Cold Spray Deposition Characteristic and Bonding of CrMnCoFeNi High Entropy Alloy, *Surf. Coat. Technol.*, 2021, **425**, p 127748.
15. S. Yin, J. Cizek, C. Chen, R. Jenkins, G. O'Donnell, and R. Lupoi, Metallurgical Bonding between Metal Matrix and Core-Shelled Reinforcements in Cold Sprayed Composite Coating, *Scripta Mater.*, 2020, **177**, p 49-53.
16. W. Sun, A.W.-Y. Tan, A. Bhowmik, F. Xue, I. Marinescu, and E. Liu, Evaluation of Cold Sprayed Graphene Nanoplates-Inconel 718 Composite Coatings, *Surf. Coat. Technol.*, 2019, **378**, p 125065.
17. Y. Zhang, J. Michael Shockley, P. Vo, and R.R. Chromik, Tribological Behavior of a Cold-Sprayed Cu-MoS2 Composite Coating During Dry Sliding Wear, *Tribol. Lett.*, 2016, **62**(1), p 9. https://doi.org/10.1007/s11249-016-0646-2
18. Y. Zhang, Y. Epshteyn, and R.R. Chromik, Dry Sliding Wear Behaviour of Cold-Sprayed Cu-MoS_2 and Cu-MoS_2-WC Composite Coatings: The Influence of WC, *Tribol. Int.*, 2018, **123**, p 296-306. https://doi.org/10.1016/j.triboint.2017.12.015
19. K. Spencer, D.M. Fabijanic, and M.-X. Zhang, The Use of Al-Al_2O_3 Cold Spray Coatings to Improve the Surface Properties of Magnesium Alloys, *Surf. Coat. Technol.*, 2009, **204**(3), p 336-344. https://doi.org/10.1016/j.surfcoat.2009.07.032
20. X. Qiu, N.U.H. Tariq, J. Wang, J. Tang, L. Gyansah, Z. Zhao, and T. Xiong, Microstructure, Microhardness and Tribological Behavior of Al_2O_3 Reinforced A380 Aluminum Alloy Composite Coatings Prepared by Cold Spray Technique, *Surf. Coat.*

Technol., 2018, **350**, p 391-400. https://doi.org/10.1016/j.surfcoat.2018.07.039
21. D. Yang, F. Qiu, Q. Zhao, L. Wang, and Q. Jiang, The Abrasive Wear Behavior of Al2014 Composites Reinforced with Ti5Si3-Coated SiCP, *Tribol. Int.*, 2017, **112**, p 33-41. https://doi.org/10.1016/j.triboint.2017.03.022
22. S. Tang, S. Shao, H. Liu, F. Jiang, D. Fu, H. Zhang, and J. Teng, Microstructure and Mechanical Behaviors of 6061 Al Matrix Hybrid Composites Reinforced with SiC and Stainless Steel Particles, *Mater. Sci. Eng. A*, 2021, **804**, p 140732. https://doi.org/10.1016/j.msea.2021.140732
23. P. Samal, P.R. Vundavilli, A. Meher, and M.M. Mahapatra, Recent Progress in Aluminum Metal Matrix Composites: A Review on Processing, Mechanical and Wear Properties, *J. Manuf. Process.*, 2020, **59**, p 131-152. https://doi.org/10.1016/j.jmapro.2020.09.010
24. D. Shechtman, I. Blech, D. Gratias, and J.W. Cahn, Metallic Phase with Long-Range Orientational Order and No Translational Symmetry, *Phys. Rev. Lett.*, 1984, **53**(20), p 1951-1953.
25. E. Huttunen-Saarivirta, Microstructure, Fabrication and Properties of Quasicrystalline Al-Cu-Fe Alloys: A Review, *J. Alloy. Compd.*, 2004, **363**(1-2), p 154-178.
26. J.M. Dubois, So Useful, Those Quasicrystals, *Isr. J. Chem.*, 2011, **51**(11-12), p 1168-1175.
27. T.P. Yadav and N.K. Mukhopadhyay, Quasicrystal: A Low-Frictional Novel Material, *Curr. Opin. Chem. Eng.*, 2018, **19**, p 163-169.
28. K. Lee, J. Hsu, D. Naugle, and H. Liang, Multi-Phase Quasicrystalline Alloys for Superior Wear Resistance, *Mater. Design,* 2016, **108**, p 440-447.
29. D.A. Rabson, Toward Theories of Friction and Adhesion on Quasicrystals, *Progress Surf. Sci.,* 2012, **87**(9-12), p 253-271.
30. B.A. de Silva GuedesLima, R. Medeiros Gomes, S.J. Guedes de Lima, D. Dragoe, M.G. Barthes-Labrousse, R. Kouitat-Njiwa, and J.M. Dubois, Self-Lubricating, Low-Friction, Wear-Resistant Al-Based Quasicrystalline Coatings, *Sci. Technol. Adv. Mater.*, 2016, **17**(1), p 71-79.
31. C. Wang, Z. Li, M.O. Iefimov, and B.N. Mordyuk, Protection of AA2024 Alloy against Wear and Corrosion by HVAF Sprayed AlCuFe Coating, *Surf. Eng.*, 2023, **39**, p 1-9. https://doi.org/10.1080/02670844.2023.2242116
32. W. Wolf, G.Y. Koga, R. Schulz, S. Savoie, C.S. Kiminami, C. Bolfarini, and W.J. Botta, Wear and Corrosion Performance of Al-Cu-Fe-(Cr) Quasicrystalline Coatings Produced by HVOF, *J. Therm. Spray Technol.*, 2020, **29**(5), p 1195-1207.
33. K. Lee, Y. Chen, W. Dai, D. Naugle, and H. Liang, Design of Quasicrystal Alloys with Favorable Tribological Performance in View of Microstructure and Mechanical Properties, *Mater. Des.*, 2020, **193**, p 108735. https://doi.org/10.1016/j.matdes.2020.108735
34. W. Wolf, F.G. Coury, M.J. Kaufman, C. Bolfarini, C.S. Kiminami, and W.J. Botta, The Formation of Quasicrystals in Al-Cu-Fe-(M=Cr, Ni) Melt-Spun Ribbons, *J. Alloys Compounds*, 2018, **731**, p 1288-1294.
35. W. Wolf, C. Bolfarini, C.S. Kiminami, and W.J. Botta, Recent Developments on Fabrication of Al-matrix Composites Reinforced with Quasicrystals: From Metastable to Conventional Processing, *J. Mater. Res.*, 2021, **36**(1), p 281-297.
36. Y. Shadangi, S. Sharma, V. Shivam, J. Basu, K. Chattopadhyay, B. Majumdar, and N.K. Mukhopadhyay, Fabrication of Al-Cu-Fe Quasicrystal Reinforced 6082 Aluminium Matrix Nanocomposites through Mechanical Milling and Spark Plasma Sintering, *J. Alloys Compounds*, 2020, **828**, p 154258.
37. T.J. Watson, A. Nardi, A.T. Ernst, I. Cernatescu, B.A. Bedard, and M. Aindow, Cold Spray Deposition of an Icosahedral-Phase-Strengthened Aluminum Alloy Coating, *Surf. Coat. Technol.*, 2017, **324**, p 57-63. https://doi.org/10.1016/j.surfcoat.2017.05.049
38. M. Hishida, M. Fujita, and K. Sakaki, Investigation of Aluminum Coating with Dispersed Nanoscale Quasicrystalline Particles Produced by Cold Spray, (Las Vegas, Nevada, USA), 2009, p 296-301, doi:https://doi.org/10.31399/asm.cp.itsc2009p0296.
39. R. Jafari, J. Kiilakoski, M. Honkanen, M. Vippola, and H. Koivuluoto, Wetting Behavior and Functionality Restoration of Cold-Sprayed Aluminum-Quasicrystalline Composite Coatings, *J. Therm. Spray Technol.*, 2023, **32**, p 609-626.
40. X. Guo, J. Chen, H. Yu, H. Liao, and C. Coddet, A Study on the Microstructure and Tribological Behavior of Cold-Sprayed Metal Matrix Composites Reinforced by Particulate Quasicrystal, *Surf. Coat. Technol.*, 2015, **268**, p 94-98.
41. N.W. Khun, R.T. Li, K. Loke, and K.A. Khor, Effects of Al-Cr-Fe Quasicrystal Content on Tribological Properties of Cold-Sprayed Titanium Composite Coatings, *Tribol. Trans.*, 2015, **58**(4), p 616-624.
42. J.F. Archard, Contact and Rubbing of Flat Surfaces, *J. Appl. Phys.*, 1953, **24**(8), p 981-988.
43. H.M. Rietveld, Line Profiles of Neutron Powder-Diffraction Peaks for Structure Refinement, *Acta Crystallogr. A*, 1967, **22**(1), p 151-152.
44. N.M. Siddesh Kumar, Dhruthi, G.K. Pramod, P. Samrat, and M. Sadashiva, A Critical Review on Heat Treatment of Aluminium Alloys, *Mater. Today Proc.*, 2022, **58**, p 71-79. https://doi.org/10.1016/j.matpr.2021.12.586
45. T. Jiang, N.U.H. Tariq, X. Qiu, Q. Zhang, L. Li, and J. Du, An Effective Approach to Improve Microstructure and Tribological Properties of Cold Sprayed Al Alloys, *Rev. Adv. Mater. Sci.*, 2023, **62**(1), p 20230314. https://doi.org/10.1515/rams-2023-0314
46. A.-P. Tsai, A. Inoue, and T. Masumoto, New Quasicrystals in Al65Cu20M15 (M = Cr, Mn or Fe) Systems Prepared by Rapid Solidification, *J. Mater. Sci. Lett.*, 1988, **7**(4), p 322-326.
47. A. Loganathan, S. Rengifo, A.F. Hernandez, C. Zhang, and A. Agarwal, Effect of Nanodiamond Reinforcement and Heat-Treatment on Microstructure, Mechanical and Tribological Properties of Cold Sprayed Aluminum Coating, *Surf. Coat. Technol.*, 2021, **412**, p 127037.
48. M.R. Rokni, C.A. Widener, O.C. Ozdemir, and G.A. Crawford, Microstructure and Mechanical Properties of Cold Sprayed 6061 Al in As-Sprayed and Heat Treated Condition, *Surf. Coat. Technol.*, 2017, **309**, p 641-650. https://doi.org/10.1016/j.surfcoat.2016.12.035
49. D. Seo, M. Sayar, and K. Ogawa, SiO_2 and $MoSi_2$ Formation on Inconel 625 Surface via SiC Coating Deposited by Cold Spray, *Surf. Coat. Technol.*, 2012, **206**(11-12), p 2851-2858. https://doi.org/10.1016/j.surfcoat.2011.12.010
50. O. Meydanoglu, B. Jodoin, and E.S. Kayali, Microstructure, Mechanical Properties and Corrosion Performance of 7075 Al Matrix Ceramic Particle Reinforced Composite Coatings Produced by the Cold Gas Dynamic Spraying Process, *Surf. Coat. Technol.*, 2013, **235**, p 108-116. https://doi.org/10.1016/j.surfcoat.2013.07.020
51. S.A. Alidokht, P. Manimunda, P. Vo, S. Yue, and R.R. Chromik, Cold Spray Deposition of a Ni-WC Composite Coating and Its Dry Sliding Wear Behavior, *Surf. Coat. Technol.*, 2016, **308**, p 424-434. https://doi.org/10.1016/j.surfcoat.2016.09.089
52. G. Munday, J. Hogan and A. McDonald, on the Microstructure-Dependency of Mechanical Properties and Failure of Low-Pressure Cold-Sprayed Tungsten Carbide-Nickel Metal Matrix Composite Coatings, *Surf. Coat. Technol.*, 2020, **396**, p 125947. https://doi.org/10.1016/j.surfcoat.2020.125947

53. R.R. Chromik, S.A. Alidokht, J.M. Shockley, and Y. Zhang, Tribological coatings prepared by cold spray, *Cold-Spray Coat. Recent Trends Future Perspect.*, 2017, p 321-348.
54. J.M. Shockley, S. Descartes, P. Vo, E. Irissou, and R.R. Chromik, The Influence of Al_2O_3 Particle Morphology on the Coating Formation and Dry Sliding Wear Behavior of Cold Sprayed Al-Al_2O_3 Composites, *Surf. Coat. Technol.*, 2015, **270**, p 324-333. https://doi.org/10.1016/j.surfcoat.2015.01.057
55. E. Irissou, J.-G. Legoux, B. Arsenault, and C. Moreau, Investigation of Al-Al_2O_3 Cold Spray Coating Formation and Properties, *J. Therm. Spray Tech.*, 2007, **16**(5-6), p 661-668. https://doi.org/10.1007/s11666-007-9086-8
56. A. Kumar, R. Kant, and H. Singh, Tribological Behavior of Cold-Sprayed Titanium/Baghdadite Composite Coatings in Dry and Simulated Body Fluid Environments, *Surf. Coat. Technol.*, 2021, **425**, p 127727. https://doi.org/10.1016/j.surfcoat.2021.127727
57. R. Cortés, M.Á. Garrido-Maneiro, H. Koivuluoto, G. Bolelli, S. Morelli, V. Testa, L. Lusvarghi, J. Kondas, and P. Poza, Local Wear Resistance of Inconel 625 Coatings Processed by Different Thermal Techniques: A Comparative Study, *Surf. Coat. Technol.*, 2023, **470**, p 129831. https://doi.org/10.1016/j.surfcoat.2023.129831